Partial and differential photoionization cross sections of Cl and Br

F. Robicheaux and Chris H. Greene
Department of Physics and The Joint Institute for Laboratory Astrophysics, University of Colorado, Boulder, Colorado 80309-0440
(Received 22 June 1992)

Partial and differential cross sections are calculated for Cl and Br near the $nsnp^5$ thresholds. We compare our calculations with experiment, obtaining good agreement over part of the energy range. The autoionizing structure is well reproduced, but the slowly evolving direct contribution to the photoionization cross section does not have the correct shape. Most of the discrepancies with experiment in the autoionizing part of the spectrum appear to derive from our neglect of doubly excited resonances in the calculations. This possibility points to the importance of an accurate theoretical description of doubly excited states of open-shell atoms. The similarity of the Cl and Br spectra in this energy range is not as pronounced as their similarity near the ns^2np^4 thresholds.

PACS number(s): 32.80.Fb, 32.80.Dz, 31.20.Di

INTRODUCTION

In an earlier paper [1] we calculated the total photoionization cross section for the halogen atoms F, Cl, Br, and I below the $ns^2np^4\,{}^1S$ threshold where the autoionizing structure is important. Generally good agreement with the available experimental data was found, although the agreement deteriorated for iodine. Due to the restricted energy region treated, Ref. [1] examined almost exclusively the photoabsorption from the outer p shell of the neutral halogen atoms (which have the valence structure $ns^2np^5\,{}^2P_{3/2}$). In this paper we describe the results of eigenchannel R-matrix calculations for Cl and Br in the autoionizing region below the $nsnp^5\,{}^3P$ thresholds and below the $nsnp^5\,{}^1P$ threshold. We compare our results to the recent experiments of van der Meulen and co-workers [2,3]. We also compare our total cross section for Cl over a larger energy range to the experiment of Samson, Shefer, and Angel [4]. These calculations provide a more sensitive test of our procedures because we are now comparing our results to partial cross sections and differential partial cross sections. We obtain excellent agreement with the experimental results over part of the spectral range. The discrepancies with experiment are found to be caused primarily by our omission of doubly excited states from the calculation. The theoretical description of these doubly excited states remains an important unresolved problem.

The ground states of Cl and Br are labeled $ns^2np^5\,{}^2P_{3/2}$ with $n=3$ for Cl and $n=4$ for Br. In a photoabsorption process, a p electron can be excited from the core into d or s waves, and an s electron can be excited from the core into p waves. The important channels for photoionization are $ns^2np^4\,({}^3P,{}^1D,{}^1S)\epsilon d$ or ϵs and $nsnp^5({}^3P^o,{}^1P^o)\epsilon p$. The ns^2np^4 thresholds ($\sim$12–16 eV) are much lower in energy than the $nsnp^5$ thresholds ($\sim$24–27 eV). In Ref. [1] we studied the photoionization near the ns^2np^4 thresholds; all of the channels described there are included in this calculation but because of the large difference in threshold energies we did not include the $nsnp^5\epsilon p$-type channels in that work. In this paper we specifically focus on the energy range near the $nsnp^5$ thresholds in order to study the $nsnp^5mp$ autoionizing resonances.

CALCULATIONS

We will not describe in detail the methods which we used to calculate the atomic dynamical parameters since the procedures are identical to those in our previous paper [1].

The major numerical approximation which we use for the description of the atomic dynamics is the streamlined formulation of the eigenchannel R-matrix procedure [5]. This procedure provides a variational estimate of the logarithmic derivative of the wave function at a given energy normal to the surface of the R-matrix volume. We define the R-matrix volume by $r_i \le r_c$ (i.e., all electrons confined to radii less than r_c) with r_c being 9 a.u. for the calculations reported here. The wave function is constructed as a superposition of basis functions, $\psi_{E\beta}=\sum_i y_i(\mathbf{r})C_{i\beta}(E)$ and has normal derivative $\partial\psi_{E\beta}/\partial n=-b_\beta(E)\psi_{E\beta}$. We include basis functions representing strong correlations as well as scattering-type basis functions in the "closed" portion of our basis set. As in Ref. [1] we only solve the Hamiltonian for the seven valence electrons, taking into account the inert inner core electrons through a screened Coulomb potential and a one- and two-electron polarizability potential.

The eigenchannel R-matrix approach provides the logarithmic derivative of the wave function at a given energy normal to the surface of the R-matrix volume. This information together with the value of the wave function at the surface completely determines the wave function everywhere outside of the R-matrix volume. The wave function outside can be written in the form

$$\psi_i=\mathcal{A}\sum_j \Phi_j^{(LS)}(\Omega)[f_j(r)\delta_{ji}-g_j(r)K_{ji}^{(LS)}]\ . \tag{1}$$

where $\mathcal{A}$ is the antisymmetrization operator (which has

no practical effect at $r > r_c$ since the outermost electron no longer overlaps the core electrons), $\Phi_j^{(LS)}(\Omega)$ represents the target function and the LS coupling of the target's angular momenta with that of the outer electron to give L and S, and $\underline{K}^{(LS)}$ is the short-range reaction matrix. Open and closed channels are included in Eq. (1); thus the ψ_i contain terms which are exponentially diverging at $r \to \infty$. The reaction matrix in Eq. (1) has the superscript LS to denote that it depends on the total spin and orbital angular momenta. $\underline{K}^{(LS)}$ is a completely nonrelativistic quantity. Each of the reaction matrices constitutes one block of a larger block-diagonal total reaction matrix,

$$\underline{K}_{LS} = \begin{bmatrix} \underline{K}^{(LS)} & 0 & \cdots \\ 0 & \underline{K}^{(L'S')} & \cdots \\ \vdots & \vdots & \ddots \end{bmatrix} . \tag{2}$$

The block-diagonal nature of $\underline{K}_{LS}$ is strictly an approximation, the error (which should be small) being due to our neglect of relativistic effects within the R-matrix volume.

J_cJ_{cs} COUPLING

We only give a brief sketch of the physical ideas motivating the frame transformation, referring the reader to Refs. [1], [6], and [7] for details. The frame transformation allows us to transform our nonrelativistic dynamical parameters into a form in which spin-orbit effects are incorporated. We differ from most previous studies in that we transform to J_cJ_{cs} coupling [8] instead of jj coupling, but this is only a difference in technical detail.

The spin-orbit interaction causes a coupling between states of different L and S but the same J. We ignore this coupling (when all of the electrons are within the reaction volume) because it has only a small effect on the short-range dynamics. However, when the outer electron leaves the atom, the rate of phase accumulation at large distances (and even whether it is bound or escapes to infinity) depends crucially on the energy of the target state it leaves behind. The energy of the target state does not depend on L_c and S_c alone but on the total angular momentum of the core, J_c. Below we give a brief description of how we incorporate this effect (see Refs. [1,6,7] for a fuller derivation).

In most of the previous calculations, the effect of the fine-structure splitting of thresholds was accounted for by applying an LS to jj frame transformation to the dynamical parameters (reaction matrices, dipole matrix elements, etc.) and using the experimentally determined threshold energies in the resulting multichannel quantum-defect-theory (MQDT) equations. However, the choice of final-state angular momenta couplings is not unique. The only requirement is that the total orbital angular momentum of the core, L_c, must be coupled to the total spin of the core, S_c, to give the total angular momentum of the core, J_c; the reason for this is that the threshold energies depend on J_c.

Instead of jj coupling we use J_cJ_{cs} coupling [8], which takes advantage of the fact that the formula for the β parameter is incoherent in J_c and J_{cs} [9]. In J_cJ_{cs} coupling the angular momenta and spin of the core and outer electron is represented by the ket: $|\{[(L_cS_c)J_cs]J_{cs}l_o\}J\rangle$, where l_o is the orbital angular momentum of the outer electron and $s = \frac{1}{2}$ is the spin of the outer electron. This ket conveys the information that the total orbital angular momentum of the core is coupled to the total spin of the core to give the total angular momentum of the core; the total angular momentum of the core is coupled to the spin of the outer electron to give J_{cs}; J_{cs} is coupled to the orbital angular momentum of the outer electron to give the total angular momentum, J, of the atom. However, when all of the electrons are near the core, the dynamics can be described much better by LS coupling which is represented by the ket: $|[(L_cl_o)L(S_cs)S]J\rangle$. This ket conveys the information that the total orbital angular momentum of the core is coupled to the orbital angular momentum of the "outer" electron to give L and the total spin of the core is coupled to the spin of the outer electron to give S; L is then coupled to S to give the total angular momentum, J, of the atom.

The reaction matrix in J_cJ_{cs} coupling is obtained from the LS-coupled K_{LS} matrix by a simple orthogonal transformation. The transformation matrix

$$U_{J_cJ_{cs},LS} = \langle \{[(L_cS_c)J_cs]J_{cs}l_0\}J|[(L_cl_o)L(S_cs)S]J\rangle \tag{3}$$

is simply the projection of one type of coupling onto the other which involves the product of two 6-j coefficients [8]. Explicitly,

$$\underline{K}_{J_cJ_{cs},J_c'J_{cs}'} = \underline{U}\,\underline{K}_{LS}\underline{U}^{\dagger} , \tag{4}$$

$$\underline{d}_{J_cJ_{cs}} = \underline{d}_{LS}\underline{U}^{\dagger} . \tag{5}$$

This is of course an approximation which is accurate so long as $\underline{K}_{LS}$ does not appreciably vary over an energy range comparable to the fine-structure splittings of the core. The ith independent solution outside of the R-matrix volume can be written in the form

$$\psi_i = \mathcal{A} \sum_j \Phi_j^{J_cJ_{cs}}(\Omega)[f_j(r)\delta_{ji} - g_j(r)K_{ji}] , \tag{6}$$

where $\Phi_j^{J_cJ_{cs}}$ represents the target function and the J_cJ_{cs} coupling of the target's total angular momentum to the spin and angular momentum of the outer electron and K_{ij} is the reaction matrix of Eq. (4) with the J_cJ_{cs} subscripts suppressed.

In Ref. [1], we found that it is necessary to also include a "dynamical" frame transformation. The spin-orbit interaction splits levels of the same L_c and S_c but different J_c and *mixes* states with the same J_c but different L_c and S_c. For example, the $ns^2np^4\,{}^3P_2^e$ state mixes with the $ns^2np^4\,{}^1D_2^e$ state. We obtained the mixing angle by fitting Slater overlap integrals of the spin-orbit interaction to the energy levels. This procedure will not work for the odd target states because they contain a very large admixture of $ns^2np^3n\bar{d}$. Since we could not obtain the mixing angle, we did not apply *any* dynamical frame transformation to the ${}^3P_1^o$ and ${}^1P_1^o$ states. For the even states the mixing angle is small, so we do not expect large errors to

occur because we have ignored the dynamical frame transformation. (We needed the dynamical frame transformation in Ref. [1] because there were some states which would not ionize without it.)

PARTIAL AND DIFFERENTIAL CROSS SECTIONS

The reaction matrix and the reduced dipole matrix elements of Eqs. (4) and (5) are not the physical $\underline{K}$ and $\underline{d}$ if any of the channels are closed (i.e., the electron cannot escape to infinity in one or more of the channels). We now use the techniques of MQDT to superpose the ψ_i of Eq. (6) in such a way that the part of the wave function in each of the closed channels decays to zero at $r\rightarrow\infty$ and is energy normalized in the open channels [10]. The ρth independent solution has a common eigenphase shift, τ_ρ, in each of the open channels. The resulting wave function has the form

$$\psi_\rho^J=\sum_{i\in o,c}\psi_i^J A_{i\rho}^J$$
$$=\mathcal{A}\sum_{i\in o}\Phi_i^{J_c J_{cs}}(\Omega)[f_i(r)\cos\pi\tau_\rho^J-g_i(r)\sin\pi\tau_\rho^J]T_{i\rho}^J\ , \quad r\rightarrow\infty \tag{7}$$

and the reduced dipole matrix elements between the initial state and the collision eigenchannel solutions Eq. (7) are

$$d_\rho^J=\sum_{i\in o,c}d_i^J A_{i\rho}^J \tag{8}$$

with $\sum_{i\in o,c}$ to be interpreted as a sum over open and closed channels while $\sum_{i\in o}$ implies a sum only over open channels. The τ_ρ^J and $T_{i\rho}^J$ are the eigenphase shifts and eigenvectors of the physical reaction matrix when the electrons are coupled to total angular momentum J, with normalization such that $TT^\dagger=1$.

The d_ρ^J of Eq. (8) are real reduced dipole matrix elements which govern the transition from the ground state to the real wave function ψ_ρ^J of Eq. (7). This standing wave is not the wave function which corresponds to an electron leaving the ion in a specific target state, nor does it represent an electron moving in a specific direction. To obtain partial cross sections and differential partial cross sections, we need to find the dipole matrix elements between the ground state and the wave function obeying the "incoming-wave boundary conditions" as discussed by Starace [11]. The wave function representing an electron leaving the ion behind in the specific state $\Phi_j^{J_c J_{cs}}$ is

$$\Psi_j^{J-}=\sum_\rho\psi_\rho^J T_{j\rho}^J\exp i(l_o^j\pi/2-\pi\tau_\rho^J-\sigma_j)\ , \tag{9}$$

where σ_j is the Coulomb phase shift in channel j, $\sigma_j=\arg\Gamma(l_o^j+1-i/\sqrt{2\varepsilon_j})$, and $\varepsilon_j=E-E_j$ is in atomic units. The full expression of $\Phi_j^{J_c J_{cs}}$ in terms of all of its components is $|\Phi_j^{J_c J_{cs}}\rangle=|\phi_j\rangle|([J_c^j s]J_{cs}^j l_o^j)J^j\rangle$ with $|\phi_j\rangle$ being the target state j with energy E_j and total angular momentum J_c^j. The second ket indicates $J_c J_{cs}$ coupling, i.e., the total angular momentum of the core, J_c^j, is coupled to the spin of the outer electron to give J_{cs}^j, and J_{cs}^j is coupled to the orbital angular momentum of the outer electron l_o^j to give the total angular momentum, J^j. The reduced dipole matrix elements, $D_i^{J-}=\langle\Psi_0^{J_0}||r^{(1)}||\Psi_i^{J-}\rangle$, connecting the initial state to these wave functions are

$$D_j^{J-}=\sum_\rho d_\rho^J T_{j\rho}^J\exp i(l_o^j\pi/2-\pi\tau_\rho^J-\sigma_j)\ . \tag{10}$$

These D_j^{J-} are proportional to the quantity $\langle j_2 l|S(J)|j',j_r\rangle$ of Eq. (5) in Ref. [9].

If the incident light is polarized in the direction $\hat{\mathbf{a}}$ (i.e., the dipole interaction in length gauge is proportional to $\hat{\mathbf{a}}\cdot\mathbf{r}=\sum_q a_q^* r_q$, where $\hat{\mathbf{a}}\cdot\hat{\mathbf{a}}=1$), the differential partial cross section for leaving the ion in state ϕ_j (which is only the ionic part of $\Phi_j^{J_c J_{cs}}$) is

$$\frac{d\sigma_j}{d\Omega}=\frac{4\pi^2\alpha\omega}{[J_g]^2\sqrt{4\pi}}\sum_{i,k}(-1)^{J_{cs}^i+J_g+J^i+J^k}D_i^{J_i-}D_k^{J_k-*}\langle\phi_j|\phi_i\rangle\langle\phi_j|\phi_k\rangle\langle J_{cs}^i|J_{cs}^k\rangle[l_o^i][l_o^k]$$
$$\times[J^i][J^k]\sum_l[l]\{Y_l(\hat{\mathbf{k}})(aa)^l\}_0^0\begin{Bmatrix}l_o^i & l_o^k & l\\ 0 & 0 & 0\end{Bmatrix}\begin{Bmatrix}l & J^i & J^k\\ J_{cs}^i & l_o^k & l_o^i\end{Bmatrix}\begin{Bmatrix}1 & l & 1\\ J^k & J_g & J^i\end{Bmatrix}\ , \tag{11}$$

where the symbol $[L]\equiv\sqrt{2L+1}$, α is the fine-structure constant, J_g is the total angular momentum of the ground state, and the symbol

$$\{Y_l(\hat{\mathbf{k}})(aa)^l\}_0^0\equiv\sum_\mu(-1)^\mu(00|l-\mu,l\mu)Y_{l-\mu}(\hat{\mathbf{k}})(aa)_\mu^l$$

and

$$(aa)_\mu^l\equiv\sum_{q,\bar{q}}(l\mu|1-q,1\bar{q})(-1)^q a_q^* a_{\bar{q}}\ .$$

The coupling $\{Y_l(\hat{\mathbf{k}})(aa)^l\}_0^0$ clearly shows that the differential cross section is unaffected if the polarization of the light and the detector are rotated in the same direction through the same angle and that the maximum angular harmonic in the differential cross section is $\mathrm{Re}[Y_{2m}(\Omega)]$. $(lm|l_1m_1,l_2m_2)$ is the Clebsch-Gordan coefficient equivalent to the $(l_1l_2lm|l_1m_1,l_2m_2)$ of Edmonds [12]. $\langle\phi_i|\phi_j\rangle$ does not equal δ_{ij}; it equals 1 when $E_i=E_j$ and $J_c^i=J_c^j$ and equals 0 otherwise. For example, we can have channel $j=3$ with the quantum numbers

$|\phi_j\rangle = |^3P^e_2\rangle$, $J^j_c = 2$, $J^j_{cs} = \frac{3}{2}$, $l^j_o = 2$, and $J^j = \frac{5}{2}$ and channel $j = 9$ with the quantum numbers $|\phi_j\rangle = |^3P^e_2\rangle$, $J^j_c = 2$, $J^j_{cs} = \frac{3}{2}$, $l^j_o = 0$, and $J^j = \frac{3}{2}$. For this definition of channels 3 and 9, $\langle\phi_3|\phi_9\rangle = 1$. The symbol $\langle J^j_{cs}|J^i_{cs}\rangle$, which equals 1 if $J^j_{cs} = J^i_{cs}$ and 0 otherwise, insures an incoherent summation over the J_{cs} quantum numbers. For the definition of channels 3 and 9 above, $\langle J^3_{cs}|J^9_{cs}\rangle = 1$. Equation (11) results from the atomic state being unpolarized and thus we average over the ground-state magnetic quantum number M_g. We also sum over the projection of J_{cs} on the z axis, M_{cs}, because it is not observed. When adding the contributions of different M_{cs}, we are implicitly summing over the magnetic quantum number of the core, M_c, and the magnetic quantum number of the outgoing electron. If either of these two quantities are observed, Eq. (11) no longer applies.

If the light is linearly polarized, we can take the direction of polarization to be the z axis giving $a_0 = 1$. For this case, $(aa)^l_\mu = \delta_{\mu 0}(\sqrt{2}\delta_{l2} - \delta_{l0})/\sqrt{3}$. Therefore, for linearly polarized light the differential partial cross section can be written as

$$\frac{d\sigma_j}{d\Omega} = \sigma_j[1 + \beta_j P_2(\cos\theta)]/4\pi \ , \tag{12}$$

where θ is the angle between the electron detector and the polarization of the light, σ_j is the partial cross section, and β_j is the asymmetry parameter. Because σ_j and β_j involve additional coherences, comparing σ_j and β_j to experiment provides a much more stringent test of the calculations than is obtained by comparing only the total cross section, $\sum_j \sigma_j$, to experiment.

CONSTRUCTING TARGET FUNCTIONS

In all of our calculations, each target function includes several configurations to ensure that the properties of the target are accurately described. The target functions for the three low-energy even-parity thresholds are the same as those in Ref. [1]. They are very nearly Hartree-Fock functions which can be labeled $ns^2np^4\,{}^3P$, ^1D, ^1S. The odd-parity thresholds which are labeled $nsnp^5\,{}^3P^o$ and $^1P^o$ have a very large admixture of ns^2np^3nd. For Cl, the amount of each CI wave function with the largest contribution to the target state of $^3P^o$ symmetry is 71% $3s3p^5$, 16% $3s^23p^3(^2D)3\bar{d}$, 8% $3s^23p^3(^2P)3\bar{d}$, and 1% $3s^23p^3(^2D)4\bar{d}$, and the amount in the target state of $^1P^o$ symmetry is 40% $3s3p^5$, 45% $3s^23p^3(^2D)3\bar{d}$, 5% $3s^23p^3(^2P)3\bar{d}$, and 5% $3s^23p^3(^2D)4\bar{d}$, where the barred d orbitals are the natural orbitals used in Ref. [1]. We will continue to label the target states by $nsnp^5$ for simplicity, although the label is misleading due to the large amount of configuration interactions.

RESULTS

The MQDT parameters cannot be as simply decomposed into alternate two-channel systems as was done in Ref. [1]. Instead of Tables I and II we give the probability matrix for the ^2P (Cl and Br) and ^2D (Cl) symmetries near the $^3P^o$ threshold. Each target state is a CI mixture of several functions as mentioned in the preceding section. The elements of this matrix are $|S_{ij}|^2$, where S_{ij} is the ij element of the smooth, short-range S matrix, some of whose indices refer to closed channels as usual in MQDT. The quantity $|S_{ij}|^2$ can be thought of as the probability of scattering from channel j into channel i in one collision with the core. With this interpretation, an electron in an isolated autoionizing resonance in a closed channel j will collide with the core approximately $N \sim 1/\sum_{i\in o}|S_{ij}|^2$ times before ionizing (assuming it decays directly to a continuum channel, rather than via another closed channel). The width divided by the spacing of Rydberg autoionizing resonances is $1/N$. Sharp autoionizing resonances occur when $N \gg 1$; resonances which are as broad as the Rydberg spacing occur when $N \sim 1$.

From Tables I and II we see that the channels which interact most strongly are those which both have the outer electron with $l = 2$ but which differ only in the core spin and orbital angular momentum. This is plausible from the fact that channels which only differ in the L_c and S_c have a large radial overlap and can interact strongly if the angular overlap is also large. One surprising feature of these tables is the very small probability of scattering from the "$3s3p^5$" $^1P^o\epsilon p$ channel into the "$3s3p^5$" $^3P^o\epsilon p$ channel. We do not know why the mixing between these two channels should be so small.

One unfortunate aspect of Tables I and II is that there does not appear to be a simple pattern of interaction between the "$nsnp^5$"ϵp channels and the $ns^2np^4\epsilon l$ channels. The only discernible pattern is the obvious one from the propensity rule for autoionizing states, i.e., resonances tend to decay into channels in which the l of the outer electron tends to remain the same or increase by 1, i.e., the ϵs channels interact most strongly with the ϵp chan-

TABLE I. Probability for scattering into different channels for the ^2P final-state symmetry of Cl and Br at an energy near the $^3P^o$ ionization threshold.

	Cl					Br				
	$^3P\epsilon s$	$^3P^o\epsilon p$	$^1P^o\epsilon p$	$^3P\epsilon d$	$^1D\epsilon d$	$^3P\epsilon s$	$^3P^o\epsilon p$	$^1P^o\epsilon p$	$^3P\epsilon d$	$^1D\epsilon d$
$^3P\epsilon s$	0.989	0.001	0.006	0.003	0.001	0.979	0.001	0.002	0.005	0.013
$^3P^o\epsilon p$	0.001	0.725	0.001	0.104	0.170	0.001	0.811	0.006	0.046	0.137
$^1P^o\epsilon p$	0.006	0.001	0.872	0.075	0.047	0.002	0.006	0.948	0.030	0.015
$^3P\epsilon d$	0.003	0.104	0.074	0.146	0.674	0.005	0.046	0.030	0.420	0.500
$^1D\epsilon d$	0.001	0.170	0.047	0.674	0.107	0.013	0.137	0.015	0.500	0.335

TABLE II. Probability for scattering into different channels for the ^2D final-state symmetry of Cl at an energy near the $^3P^o$ ionization threshold.

	$^1D\epsilon s$	$^3P^o\epsilon p$	$^1P^o\epsilon p$	$^3P\epsilon d$	$^1D\epsilon d$	$^1S\epsilon d$
$^1D\epsilon s$	0.977	0.006	0.010	0.002	0.004	0.001
$^3P^o\epsilon p$	0.006	0.757	0.000	0.111	0.040	0.085
$^1P^o\epsilon p$	0.010	0.000	0.821	0.081	0.078	0.010
$^3P\epsilon d$	0.002	0.111	0.081	0.233	0.456	0.117
$^1D\epsilon d$	0.004	0.040	0.078	0.456	0.336	0.086
$^1S\epsilon d$	0.001	0.085	0.010	0.117	0.086	0.701

nels and the ϵp channels interact most strongly with the ϵd channels. However, at this point we do not see any simple physical reason (for example) why the probability for scattering from the $^3P^o\epsilon p$ channel into the $^{2S+1}L\epsilon d$ channels should have the values given in Tables I and II.

In Fig. 1 we plot our length and velocity results with the experimental data of Samson, Shefer, and Angel [4]. Although the overall magnitude of the results is in reasonable agreement, the shapes of the calculated and experimental cross sections are in poorer agreement. It appears that the position of the theoretical Cooper minimum is too high in energy. Our previous calculation [1] was in better agreement with this experiment (in size and shape) near the ^1S threshold $\sim$760 Å. That calculation used as many basis functions as this one to describe a much smaller energy range and therefore was more accurate.

In Figs. 2–5 we give the experimental [2] and calculated asymmetry parameters and partial cross sections for Cl. We do not give the partial cross sections to the individual $^3P_J^e$ states because the experiment did not have enough sensitivity to resolve the fine-structure components of this configuration. We only plot the length gauge cross sections to avoid clutter in the graphs. The velocity gauge cross sections were uniformly $\sim$25% smaller than the length gauge cross sections, but cross sections in the two different gauges had nearly the same shape. The asymmetry parameters were nearly identical in the two different gauges.

In the range below the $^3P^o$ threshold, we obtain very good agreement between theory and experiment, especially for the partial cross section plotted in Fig. 2. The only real discrepancy in this energy range is in the $^3P^e$ asymmetry parameter near 23.3 eV in Fig. 3(a). The experimental data displays a very sharp drop of $\sim$1 in β whereas the calculation remains flat. A small corresponding resonance in the experimental $^3P^e$ partial cross section is absent from the calculation [Fig. 2(a)]; otherwise the disagreement between experimental and calculated partial cross sections is very slight and would have probably been attributed to noise if there were not such a large disagreement in the β parameters. Because this resonance only shows up in the $^3P^e$ channel it is probably a quartet doubly excited state of the type $3s^23p^33d4p$. We

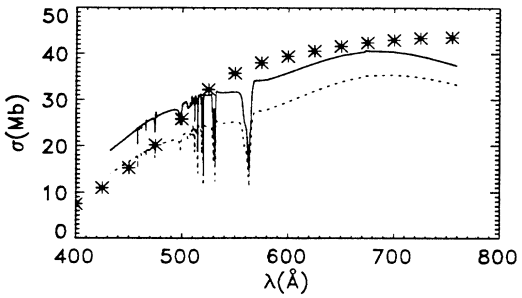

FIG. 1. Experimental and theoretical total photoionization cross section of Cl as a function of wavelength. *, experimental points of Ref. [4]; solid line, length gauge calculation; dotted line, velocity gauge calculation. The $^3P^o$ thresholds are near 505 Å and the $^1P^o$ thresholds are near 455 Å. The rest of the figures are plotted as a function of frequency with ω (eV)$\cong$12 400/λ (Å).

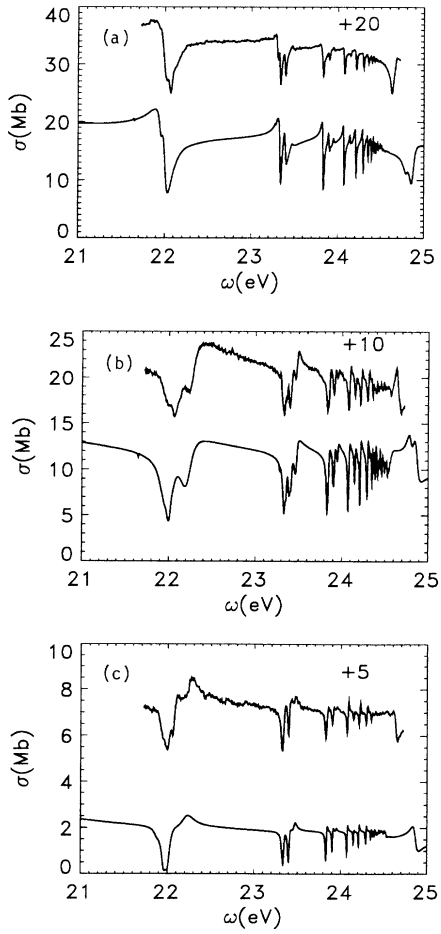

FIG. 2. Experimental and theoretical (length gauge) partial photoionization cross section of Cl near the $^3P^o mp$ autoionizing region. We have convolved the calculation with the quoted experimental resolution of 0.16 Å of Ref. [2]. (a) $^3P^e$ partial cross section (we have added 20 Mb to the experimental cross section for clarity). (b) ^1D partial cross section (we have added 10 Mb to the experimental cross section). (c) ^1S partial cross section (we have added 5 Mb to the experimental cross section). The $^3P^o$ thresholds are near 24.6 eV.

feel that it must be a doubly excited state (as opposed to a subtle effect of channel mixing) because the resonance is very sharp and in a range where the partial cross section is large.

Below the $^1P^o$ threshold the agreement is not as good. The main difference derives from the numerous extra resonances in the experimental cross sections (Fig. 4). These also are presumably doubly excited states. If they are indeed doubly excited states, it is not surprising that we cannot reproduce these structures for the simple reason that we have not put them into our calculation. The effort needed to get the positions and shapes of doubly excited resonances is probably much greater than the effort used to calculate the MQDT parameters from the $^3P^e$ threshold at 13 eV to the $^1P^o$ threshold at 27.3 eV. However, we obtain good agreement in shape and position for the experimental resonances which are in our calculation. The $4p$ autoionizing resonance is at 24.85 eV ($n^*=2.33$) in the calculation and 24.63 eV ($n^*=2.25$) in the experiment. The error in the effective quantum number is slightly larger than expected and may be due to the large CI mixing of the $^1P^o$ target state. The effort needed to converge a target state greatly magnifies the effort needed to converge a resonance attached to that state. This error is what causes the discrepancy between calculated and experimental asymmetry parameters in Fig. 5. The error in the description of this resonance appears to be only in its position, as the width and shape emerge correctly.

Reference [2] gives tables of experimental and theoretical absolute partial cross sections and asymmetry parameters of Cl at 21.218 eV. We only give the comparison of our results with the experimental values of Ref. [2] and the theoretical results of Shahabi and co-workers [13] who used the open-shell transition matrix (OSTM) method. We obtain good agreement with both the experimental and OSTM results for the partial cross sections. Our length (velocity) gauge values are 19.7 (15.6) Mb, 12.6 (10.6) Mb, and 2.3 (2.0) Mb for the $^3P^e$, ^1D, and ^1S partial cross sections compared to the experimental values [2] of 16.7±2.5, 11.7±2.5, and 2.4±0.8 Mb and

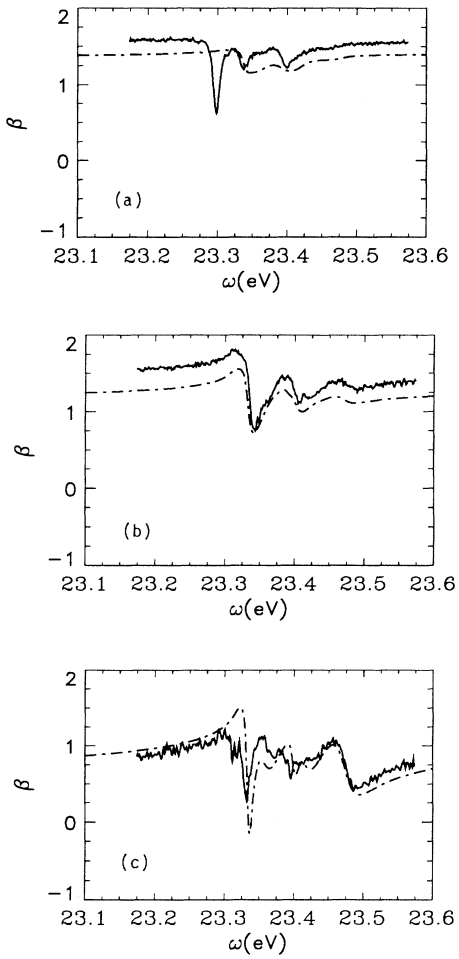

FIG. 3. Experimental (solid line) and theoretical (dashed line) (length gauge) asymmetry parameter of Cl near the $^3P^o5p$ autoionizing resonances. We have convolved the calculation with the quoted experimental resolution of 0.11 Å of Ref. [2]. (a) $^3P^e$ asymmetry parameter. (b) ^1D asymmetry parameter. (c) ^1S asymmetry parameter.

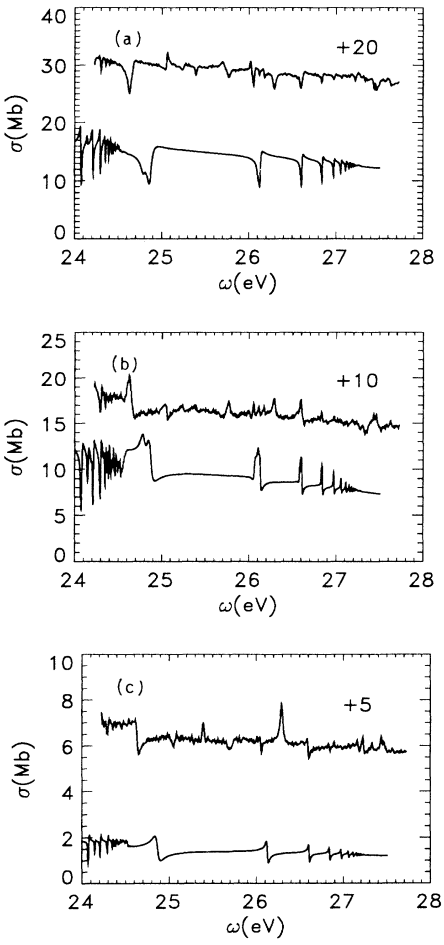

FIG. 4. Same as Figs. 2(a)–2(c) but in the $^1P^o mp$ autoionizing region. The $^1P^o$ thresholds are near 27.3 eV.

the OSTM [13(a)] values of 19.7, 13.8, and 2.4 Mb. Pan and Starace [14] predict the partial cross sections to be proportional to 9:5:1, which is in good agreement with experiment and theory; they assume that the radial one-electron dipole matrix element connecting the p-valence electron of the ground state to the outgoing s and d waves are independent of the L and S quantum numbers of the final state. Our calculated asymmetry parameters agree with the experimental results better than they do with the OSTM value. Our length (velocity) gauge values are 1.29 (1.29), 1.19 (1.18), and 0.75 (0.75) for the $^3P^e$, ^1D, and ^1S asymmetry parameters compared to the experimental values [2] of 1.48 ± 0.1, 1.29 ± 0.1, and 0.83 ± 0.1 and the OSTM [13(b)] values of 1.49, 1.20, and 1.34. We do not know the reason for the discrepancy between our value of the ^1S asymmetry parameter and that of Shahabi and coworkers. Most of the previous theoretical values lie between 1.5 and 1.8 for the ^1S asymmetry parameter.

Pan and Starace [14] also predict the ratio of photoionization cross sections for photoabsorption from the s shell, although it is not obvious that a single configuration treatment such as theirs will prove reliable in this case. That is, they assume the ion to be 100% $3s3p^5$ as compared to our findings that it is 71% $3s3p^5$ for $^3P^o$ and 40% $3s3p^5$ for $^1P^o$. Nevertheless, their relative fine-structure partial cross sections $^3P^o_J$ for photoabsorption from $3s^3 3p^5\,^3P_{3/2}$ are in the ratio 5:1:0 for $J=2,1,0$, respectively, while our values are proportional to 4.9:1.1:0.1. As they discuss, this good agreement seems to indicate an insensitivity of fine-structure branching ratios to configuration mixing in the ionic states in this case. However, their prediction for the $^1P^o$-to-$^3P^o$ partial cross section ratio is 0.25:0.75 as compared to our value of 0.12:0.88. This factor of 2 disagreement for the $^1P^o$-to-$^3P^o$ branching ratio is most likely due to the much stronger configuration mixing in the $^1P^o$ ion state. On the whole, however, taking into account both their p- and s-subshell predictions, their results are in good agreement with our more elaborate calculations.

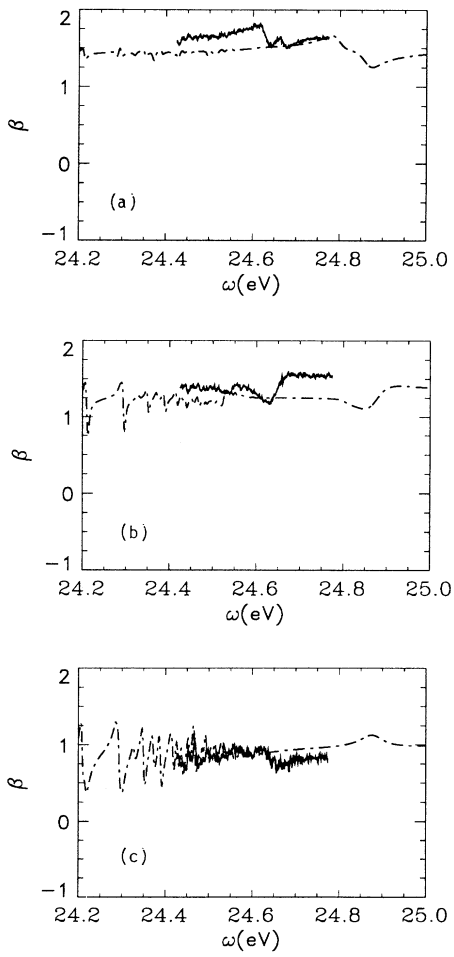

FIG. 5. Same as Figs. 3(a)–3(c) but near the $^1P^o 4p$ autoionizing resonances.

The only other study of the autoionizing resonances in the region below the $^3P^o$ and $^1P^o$ thresholds was carried out by Brown, Carter, and Kelly [15]. Their calculation was carried out in LS coupling so they were unable to reproduce the effects due to the fine-structure splitting of the $^3P^o$ threshold. Our LS results (i.e., ignoring fine-structure effects) are in very good agreement with theirs below the $^3P^o$ threshold with our quantum defects being ~ 0.03 larger (which is a negligible difference). The shapes of these resonances were also in good agreement. Below the $^1P^o$ threshold our quantum defects are in good agreement with their quantum defects. However, the shapes of the resonances differ. The total cross section near the $^1P^o np$ resonances in our calculations first slightly rises above, then dips below the background value whereas their cross section first dips below, then rises above the background value. The magnitude for the Fano q parameter was larger in their calculation.

We classified all of the $^3P^o_{J_c}$ np resonances below 24.6 eV by examining the probability for finding an electron in each of the closed channels as a function of energy. At a resonance, the probability for being in a closed channel

TABLE III. The positions and classifications of the $3s3p^5\,^3P_{J_c}\,J_{cs}5pJ$ autoionizing resonances.

Energy	Classification
23.36 eV	$J_c=2, J_{cs}=\frac{3}{2}, J=\frac{1}{2}$
23.41 eV	$J_c=1, J_{cs}=\frac{1}{2}, J=\frac{1}{2}$
23.41 eV	$J_c=1, J_{cs}=\frac{3}{2}, J=\frac{1}{2}$
23.47 eV	$J_c=0, J_{cs}=\frac{1}{2}, J=\frac{1}{2}$
23.28 eV	$J_c=2, J_{cs}=\frac{5}{2}, J=\frac{3}{2}$
23.33 eV	$J_c=2, J_{cs}=\frac{3}{2}, J=\frac{3}{2}$
23.39 eV	$J_c=1, J_{cs}=\frac{3}{2}, J=\frac{3}{2}$
23.40 eV	$J_c=1, J_{cs}=\frac{1}{2}, J=\frac{3}{2}$
23.44 eV	$J_c=0, J_{cs}=\frac{1}{2}, J=\frac{3}{2}$
23.32 eV	$J_c=2, J_{cs}=\frac{3}{2}, J=\frac{5}{2}$
23.34 eV	$J_c=2, J_{cs}=\frac{5}{2}, J=\frac{5}{2}$
23.38 eV	$J_c=1, J_{cs}=\frac{3}{2}, J=\frac{5}{2}$

peaks and the largest of the relative weights in each of those closed channels determines the classification. The resonances near 22 eV were unclassifiable in $J_c J_{cs}$ coupling, having large contributions from many closed channels. We interpret this as meaning that these resonances are nearly LS coupled; their large widths allow the resonances to overlap which also confuses the issue. In Table III we give the energies and classifications of the resonances between 23.1 and 23.6 eV. These resonances all have the character $3s3p^5\,{}^3P^o_{J_c}\,J_{cs}5pJ$ and are reasonably (about 70%) pure compared to the resonances at 22 eV. For example, the first resonance of Table III at 23.36 eV, $J=\frac{1}{2}$, was 76% ${}^3P^o_2\,J_{cs}=\frac{3}{2}$, 9% ${}^3P^o_1\,J_{cs}=\frac{1}{2}$, and 14% ${}^3P^o_1\,J_{cs}=\frac{3}{2}$. In general, the widths of the resonances are broader than the spread in energy of all the levels attached to each J_c threshold, making it impossible to distinguish all of the resonances experimentally. All that can be said experimentally is that at $\sim$23.33, $\sim$23.40, and $\sim$23.45 eV there is a cluster of $J_c=2$, $J_c=1$, and $J_c=0$ resonances. The problem with this classification of levels is especially exacerbated for those states with the same J_c and J but different J_{cs}; these states are usually very heavily mixed and nearly degenerate. The proper quantum number that should replace J_{cs} is unknown (the Hamiltonian should be nearly diagonal with respect to this quantum number). The purity of the levels increases still further for the group of resonances between 23.8 and 24.0 eV. At higher energies, a Rydberg level in one channel can be nearly degenerate with a Rydberg level in another channel which would cause large mixing between those states.

In Figs. 6 and 7 we graph the calculated and experimental [3] partial cross sections of Br below the $4s4p^5\,{}^3P^o$ thresholds. In Fig. 6 we plot the ${}^3P^e_2$ partial cross section over a larger energy range than that covered in Fig. 7. We used exactly the same choice of configurations for the Br calculation as we did for the Cl calculation with the $(n+1)s$, $(n+1)p$, $(n+1)d$, and nf orbitals of Br substituted for the ns, np, nd, and nf orbitals of Cl. It is possible we could have obtained better agreement by choosing configurations which better describe Br. All of the resonances of the calculation match features in the experiment (Fig. 6) in both size and shape. The calculated positions of the $4s4p^5\,{}^3P^o\,5p$ resonances near 21.3 eV of Figs. 6 and 7 are too high by about 0.1 eV. The calculated partial cross sections (Fig. 7) are in agreement with the experimental resonances in shape and magnitude except for

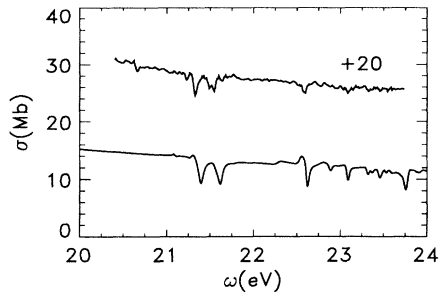

FIG. 6. Experimental and theoretical ${}^3P^e_2$ partial cross section of Br (we have added 20 Mb to the experimental cross section for clarity). The calculated length gauge cross section has been convolved with the quoted experimental resolution of 0.7 Å. The ${}^3P^o$ thresholds are near 24.1 eV.

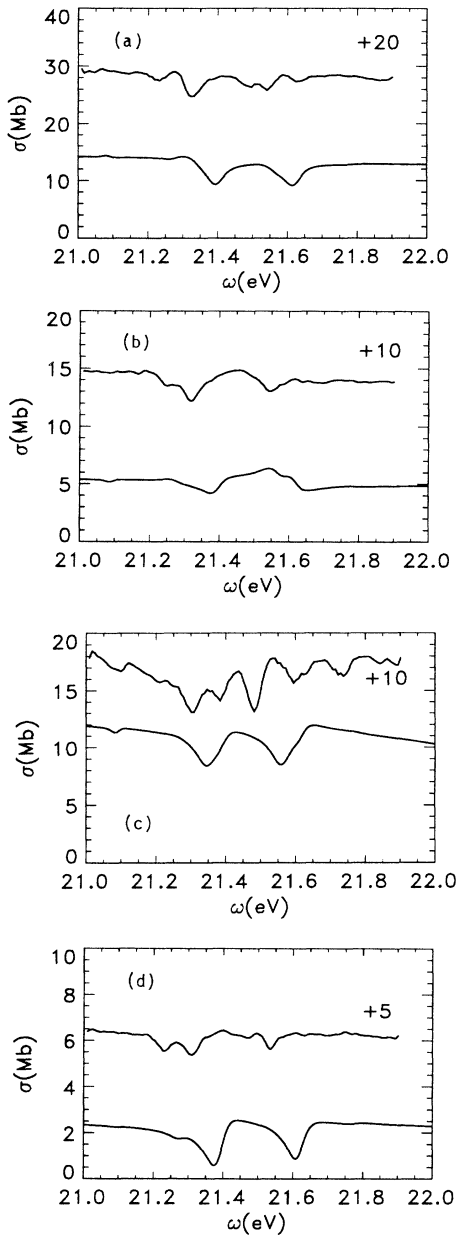

FIG. 7. Experimental and theoretical partial photoionization cross sections of Br near the ${}^3P^o5p$ autoionizing resonances. We have convolved the theoretical length gauge cross sections with the quoted experimental resolution 0.7 Å of Ref. [3]. (a) ${}^3P^e_2$ partial cross section (we have added 20 Mb to the experimental cross section). (b) ${}^3P^e_{1,0}$ partial cross section (we have added 10 Mb to the experimental cross section). (c) ${}^1D$ partial cross section (we have added 10 Mb to the experimental cross section). (d) ${}^1S$ partial cross section (we have added 5 Mb to the experimental cross section).

the ^1D partial cross section [Fig. 7(c)], which has many more structures in the experimental data. It is possible that these structures represent doubly excited resonances which are not included in the calculation. However, this seems unlikely because doubly excited resonances would probably manifest themselves in all of the partial cross sections. We do not know what could be causing the discrepancies. By comparing Figs. 2 and 6, many similarities between Cl and Br become apparent. These similarities are not as striking as those near the lower-energy thresholds. The differences between the two atoms probably derive from the larger spin-orbit splitting of the $^3P^o$ thresholds in Br; the probability matrix for Br (for the ^2P final-state symmetry) is very similar to the probability matrix of Cl (Table I).

CONCLUSIONS

We have presented calculations of the differential and partial photoionization spectra of Cl and Br in the energy range where the valence s electrons can be excited and compared them to available experimental data. Doubly excited states in this energy range were not included in the calculations and this omission appears to be responsible for most of the discrepancies with the experiment. It seems that the theoretical description of doubly excited states of multielectron atoms is an important aspect of atomic dynamics which will require considerably more effort than the present study. However, the singly excited resonances are generally well reproduced.

ACKNOWLEDGMENTS

We thank P. van der Meulen for giving us the experimental data of Refs. [2] and [3]. We also appreciate helpful conversations with A. F. Starace about theoretical aspects of this problem and with M. O. Krause and C. D. Caldwell about experimental aspects of this problem. We also thank Arlene Robey for helping us with the references for Br VII and I VII needed for Ref. [1] and this work. This research was supported by the Division of Chemical Sciences, Office of Basic Energy Sciences, Office of Energy Research, U.S. Department of Energy Grant No. DE-FG-02-90ER14145.

[1] F. Robicheaux and C. H. Greene, Phys. Rev. A **46**, 3821 (1992).
[2] P. van der Meulen, M. O. Krause, C. D. Caldwell, S. B. Whitfield, and C. A. de Lange, Phys. Rev. A **46**, 2468 (1992); J. Phys. B **24**, L573 (1991).
[3] P. van der Meulen, M. O. Krause, and C. A. de Lange, J. Phys. B **25**, 97 (1992).
[4] J. A. R. Samson, Y. Shefer, and G. C. Angel, Phys. Rev. Lett. **56**, 2020 (1986).
[5] C. H. Greene and L. Kim, Phys. Rev. A **38**, 5953 (1988).
[6] A. R. P. Rau and U. Fano, Phys. Rev. A **4**, 1751 (1971); C. M. Lee and K. T. Lu, *ibid.* **8**, 1241 (1973).
[7] L. Kim and C. H. Greene, Phys. Rev. A **36**, 4272 (1987).
[8] M. D. Lindsay, C.-J. Dai, L.-T. Cai, T. F. Gallagher, F. Robicheaux, and C. H. Greene, Phys. Rev. A **46**, 3789 (1992).
[9] U. Fano and D. Dill, Phys. Rev. A **6**, 185 (1972). We use a philosophy similar to that of Fano and Dill; however, we do not utilize their j_l quantum number.
[10] U. Fano and A. R. P. Rau, *Atomic Collisions and Spectra* (Academic, Orlando, 1986); M. J. Seaton, Rep. Prog. Phys. **46**, 167 (1983).
[11] A. F. Starace, in *Handbuch der Physik,* edited by S. Flügge and W. Mehlhorn (Springer-Verlag, Berlin, 1982), Vol. 31.
[12] A. R. Edmonds, *Angular Momentum in Quantum Mechanics* (Princeton University Press, Princeton, 1974).
[13] (a) S. Shahabi, A. F. Starace, and T. N. Chang, Phys. Rev. A **30**, 1819 (1984); (b) S. Shahabi and A. F. Starace, *ibid.* **33**, 2111 (1986).
[14] C. Pan and A. F. Starace (unpublished).
[15] E. R. Brown, S. L. Carter, and H. P. Kelly, Phys. Rev. A **21**, 1237 (1980).